Nucleon-deuteron scattering with the JISP16 potential

R. Skibiński, J. Golak, K. Topolnicki, H. Witała, Yu. Volkotrub, H. Kamada, A. M. Shirokov, R. Okamoto, K. Suzuki, and J. P. Vary

Phys. Rev. C **97**, 014002 — Published 22 January 2018

DOI: 10.1103/PhysRevC.97.014002

Nucleon-deuteron scattering with the JISP16 potential

R. Skibiński, J. Golak, K. Topolnicki, H. Witała, and Yu. Volkotrub

M. Smoluchowski Institute of Physics,
Jagiellonian University, PL-30348 Kraków, Poland

H. Kamada

Department of Physics, Faculty of Engineering,
Kyushu Institute of Technology, Kitakyushu 804-8550, Japan

A. M. Shirokov

Skobeltsyn Institute of Nuclear Physics,
Moscow State University, Moscow 119991, Russia and

Department of Physics, Pacific National University, Khabarovsk 680035, Russia

R. Okamoto and K. Suzuki

Senior Academy, Kyushu Institute of Technology, Kitakyushu 804-8550, Japan

J. P. Vary

Department of Physics and Astronomy,
Iowa State University, Ames, IA 50011-3160, USA
(Dated: November 25, 2017)

Abstract

The nucleon-nucleon J-matrix Inverse Scattering Potential JISP16 is applied to elastic nucleon-deuteron scattering and the deuteron breakup process at the laboratory nucleon energies up to 135 MeV. The formalism of the Faddeev equations is used to obtain three-nucleon scattering states. We compare predictions based on the JISP16 force with data and with results based on various two-body interactions, including the CD Bonn, the Argonne AV18, the chiral force with the semi-local regularization at the fifth order of the chiral expansion and with low-momentum interactions obtained from the CD Bonn force as well as with the predictions from the combination of the AV18 NN interaction and the Urbana IX 3N force. JISP16 provides a satisfactory description of some observables at low energies but strong deviations from data as well as from standard and chiral potential predictions with increasing energy. However, there are also polarization observables at low energies for which the JISP16 predictions differ from those based on the other forces by a factor of two. The reason for such a behavior can be traced back to the P-wave components of the JISP16 force. At higher energies the deviations can be enhanced by an interference with higher partial waves and by the properties of the JISP16 deuteron wave function. In addition, we compare the energy and angular dependence of predictions based on the JISP16 force with the results of the low-momentum interactions obtained with different values of the momentum cutoff parameter. We found that such low-momentum forces can be employed to interpret the nucleon-deuteron elastic scattering data only below some specific energy which depends on the cutoff parameter. Since JISP16 is defined in a finite oscillator basis, it has properties similar to low momentum interactions and its application to the description of nucleon-deuteron scattering data is limited to a low momentum transfer region.

PACS numbers: 21.45.-v, 13.75.Cs, 25.40.Cm

I. INTRODUCTION

Various models of the nucleon-nucleon (NN) interaction have been derived in the past. Some of them, like the Charge Dependent Bonn (CD Bonn) [1, 2] potential arise from the boson-exchange picture of nuclear interactions and aim not only at describing data but also at providing insight into the underlying physics. Other models, like the Argonne AV18 [3] potential, exploit the possible operator structure and preserve the pion exchange picture for the long-range component of the interaction while introducing a phenomenological parametrization for the short-range part. Even the most advanced models have to incorporate numerous adjustable parameters (about 40 for the CD Bonn or the AV18 models) whose values have to be fixed from NN data. Such semi-phenomenological potentials describe the NN scattering data and deuteron properties with high precision, achieving for example χ^2/data$'$99=1.35 in the case of the AV18 force and χ^2/data$'$99=1.01 for the CD Bonn model [4].

Another approach arises from the chiral effective field theory where one builds the effective nuclear potential basing on Lagrangian for nucleon and pion fields [5, 6]. So far the chiral NN interaction has been derived completely up to the fifth order of the chiral expansion (N^{4}LO) [7, 8]. Moreover, the dominant contributions at the sixth order are also known [9]. The good quality of the chiral force with the semi-local regularization [7, 8] and weak cutoff dependence of predictions was confirmed in the 3N continuum, both for strong [10] and electroweak [11] processes, as well as in nuclear structure calculations.

The JISP16 NN potential was presented ten years ago in Ref. [12]. This force was a successor of the J-matrix Inverse Scattering Potential JISP6 [13], which in turn followed the Inverse Scattering Tridiagonal Potential (ISTP) developed within the J-matrix inverse scattering formalism in [14]. Free parameters of the JISP6 force have been fixed by fitting to the NN phase shifts as well as to bound and resonance states of nuclei up to $A = 6$. Correspondingly, bound and resonance states of nuclei up to ^{16}O have been used to adjust the free parameters of its successor, the JISP16 force. Both JISP forces describe also NN scattering data with high precision, comparable to the other modern potentials, reaching $\chi^2 = 1.03(1.05)$ with the neutron-proton data'1992(1999) [15]([2]). The JISP forces assume charge independence and, regarding the NN system, only the neutron-proton scattering data and the deuteron properties have been taken into account when fixing the parameters.

An important feature of the JISP16 force is that it provides sufficient convergence of the No-Core Shell Model [16] calculations enabling accurate predictions for nuclear binding energies and spectra of excited nuclear states with established extrapolation techniques [17–19] and the ability to perform perturbative calculations of nuclear matter [20]. The description of properties of light nuclei by JISP16 is rather accurate, see Refs. [21, 22]. In particular, the accuracy of ^{14}F binding energy and spectrum predictions [23] based on this interaction was later confirmed by the first experimental study of this nucleus in Ref. [24]. The JISP16 force is also known to provide an accurate *ab initio* description of resonance energies and widths in nucleon-α scattering [25–27] and in the tetraneutron system [28]. These successful applications of the JISP16 interaction have encouraged us to test this force also in the studies of nucleon-deuteron scattering which is a well-known challenge for inter-nucleon forces [29–31].

Momentum space matrix elements of the JISP16 potential decrease quickly with increasing momenta which makes this force very useful in nuclear structure calculations. This welcome feature of NN interactions was one of the reasons for developing the so-called "low momentum interactions" $V_{\rm low\,k}$ [32–35]. The force of Refs. [32, 33], which originated from an application of the regularization group methods to soften the interaction, has also been

widely used in calculations of energy levels of various nuclei and in nuclear matter studies (see reviews [36, 37] and references therein). These methods take care about the unitarity of the transformation both in NN and many-nucleon systems. They thus preserve the description of two-nucleon (2N)[1] and 3N observables both in bound states and scattering processes with arbitrary energies. Another idea lies at the heart of the low momentum interaction obtained in Ref. [34]. There the NN force was constructed by means of a transformation which cuts off the short range (or equivalently the high momentum) part of the realistic input potential. As a consequence it retains the same description of the NN observables but only for the c.m. NN energy below the value defined by the cut off parameter.

The authors of Refs. [32, 33] recommend using the cutoff parameter around Λ=2 fm^{-1}, in contrast with Ref. [34], where the value of Λ=5 fm^{-1} was suggested. It should be emphasized that in Refs. [32–34] additional 3N forces, which appear when on-the-energy-shell equivalent low momentum 2N interactions are used in systems with more than two particles [38, 39], were omitted. It is clear that the value of Λ correlates with the energy range where the corresponding $V_{\rm low\ k}$ can be used. In the few-nucleon sector, the $V_{\rm low\ k}$ interaction constructed within the approach of Refs. [32, 33] from various models of the NN interaction, was applied in Ref. [40] to study the neutron analyzing power in elastic neutron-deuteron scattering at the neutron energy of 3 MeV, the breakup cross section in the space star (SST) configuration at E = 13 MeV and some selected observables in neutron-triton scattering at energies below 6 MeV. The application of the $V_{\rm low\ k}$ potential obtained using the method of Ref. [33] to proton-deuteron elastic scattering was presented also in Ref. [41] at low center-of-mass energies, up to 2 MeV. At these energies the used $V_{\rm low\ k}$ force (based on the AV18 with the cutoff parameters Λ equal to 2.2 fm^{-1}) delivers a very good description of the cross section and various spin observables.

To the best of our knowledge, up to now the $V_{\rm low\ k}$ potential obtained using the approach of Ref. [34] has not been used to study elastic nucleon-deuteron (Nd) scattering. We fill this gap in the present paper and show predictions for various observables in Nd scattering at the laboratory kinetic energies of the incoming nucleon ranging from 5 MeV to 135 MeV. Our results are obtained with the $V_{\rm low\ k}$ force derived with the method of Ref. [34] applied to the CD Bonn force. We use the Λ cutoff values ranging from 1.5 fm^{-1} to 5.0 fm^{-1}. Observables obtained in this way are compared with the CD Bonn predictions and with the JISP16 results. Being aware that the additional three-nucleon force should be taken into account when applying the low momentum interaction of Ref. [34] to 3N processes, we use here this interaction in order to compare it with the JISP16 force rather than to describe specific 3N data.

The role of the induced 3NF resulting from the regularization group methods has been investigated both in the nuclear structure, see e.g. Ref.[38], and at low energies in 3N scattering [40], while the role of additional 3NF accompanying the low momentum interaction of Ref. [34] has been estimated only for the ^{3}H and ^{4}He nuclei in Ref. [34]. It has been found that one can expect the contribution of additional 3NF to the triton binding energy up to 0.7 MeV, depending on the cut-off parameter value in the range above 1.0 fm^{-1}. This is approximately 50% of the contribution given by "realistic" 3NFs. Thus it is plausible to think that also in the Nd scattering process the impact of additional 3NF is smaller than the contribution of "realistic" 3NFs.

The JISP16 potential was, from the very beginning, assumed to give a good description of nuclei in absence of the many-body interactions and many-body observables have been used

[1] We use NN and 2N interchangeably with preference for the latter when warranted by the context.

to fix its parameters. Indeed, results from the structure calculations confirm this feature of the JISP16 potential. In this paper we would like to check if this observation is also valid for the 3N scattering observables. To this end we compare the predictions based on the JISP16 force with ones obtained from a Hamiltonian containing an explicit 3NF, namely by using the AV18 NN potential combined with the Urbana IX [42] 3NF. However, we are also interested in a comparison of predictions based on the JISP16 force with the results based on other models of the 2N interaction with a focus on the role of softening those interactions.

The paper is organized as follows: in the next section we shortly describe the framework of the 3N Faddeev equations. In Sec. III we discuss some properties of 2N and 3N bound states. Predictions for the Nd elastic scattering and the deuteron breakup reaction obtained, for the first time, with the JISP16 potential, and their comparison with results of calculations based on semi-phenomenological and chiral N^{4}LO potentials are shown and discussed in Sec. IV. In Sec. V we compare the JISP16 Nd scattering results with those based on the $V_{\rm low\ k}$ forces. Finally, we present our summary and conclusions in Sec. VI.

II. FORMALISM

Results for the Nd scattering presented in this work have been obtained in the framework of the Faddeev equations in momentum space. Since this formalism is nowadays one of the standard techniques to investigate 3N reactions and has been described in detail many times, we only briefly remind the reader the most fundamental steps. The interested reader can find more details, e. g., in Refs. [43–45].

In this approach, the Faddeev equation for an auxiliary state $T|\phi\rangle$ is the central equation to be solved. It reads

$$T|\phi\rangle = tP|\phi\rangle + tPG_0T|\phi\rangle + (1+tG_0)V_4^{(1)}(1+P)|\phi\rangle + (1+tG_0)V_4^{(1)}(1+P)T|\phi\rangle, \quad (2.1)$$

where the initial state $|\phi\rangle$ is composed of a deuteron and a relative momentum eigenstate of the projectile nucleon, P is a permutation operator which takes into account the identity of the nucleons and G_0 is the free 3N propagator. The 2N interaction V together with the 2N free propagator $\tilde{G}_0$ appear in the Lippmann–Schwinger equation for the 2N t-matrix

$$t = V + V\tilde{G}_0 t \ . \quad (2.2)$$

In Eq. (2.1) $V_4^{(1)}$ is that part of the 3NF which is symmetrical under the exchange of nucleons 2 and 3. When the 3NF is neglected, Eq. (2.1) reduces to

$$T|\phi\rangle = tP|\phi\rangle + tPG_0T|\phi\rangle \ . \quad (2.3)$$

We solve Eqs. (2.1) and (2.3) in the momentum space partial wave scheme. We work with the $|p,q,\alpha\rangle$ states with $p = |\,\vec{p}\,|$ and $q = |\,\vec{q}\,|$ being the magnitudes of the relative Jacobi momenta $\vec{p}$ and $\vec{q}$. Further, α represents the set of discrete quantum numbers for the 3N system in the jI-coupling

$$\alpha = \big((l,s)j;(\lambda,\frac{1}{2})I;(j,I)JM_J;(t\frac{1}{2})TM_T\big) \ . \quad (2.4)$$

Here l, s, j and t denote the orbital angular momentum, total spin, total angular momentum and total isospin of the 2-3 subsystem. Further, λ and I are the orbital and total angular

momenta of the spectator nucleon 1 with respect to the center of mass of the 2-3 subsystem. Finally, J, M_J, T and M_T are the total angular momentum of the 3N system, its projection on the quantization axis, the total 3N isospin and its projection, respectively.

It is worth noting that during solving Eqs. (2.1) or (2.3) the 2N force matrix elements, present in the t-operator, clearly interfere which can significantly affect the observables. We solve Eq. (2.3) by generating its Neumann series and summing it up by using the Padé method [44]. For results presented here we use all partial waves with $j \leq 4$ and $J \leq \frac{25}{2}$. More details about our numerical performance can be found in [44].

The JISP16 potential is initially available [46] in the harmonic oscillator (HO) basis which is used commonly in nuclear structure calculations. The matrix elements of that potential in 2N momentum space basis $|p, \tilde{\alpha}\rangle \equiv |p, (l, s)j; t\rangle$ are then given by

$$\langle p', \tilde{\alpha}'|V|p, \tilde{\alpha}\rangle = \sum_{n=0}^{n^l_{\max}} \sum_{n'=0}^{n^{l'}_{\max}} (-1)^{n+n'} i^{l'-l} R_{n'l'}(p'b) R_{nl}(pb) b^3 \langle n', l'|V_{sj}|n, l\rangle \,, \tag{2.5}$$

where n and n' are the principal quantum numbers for HO states and, due to the definition of the JISP16 interaction, $n^l_{\max} = (8-l)/2$ or $(9-l)/2$ depending on the parity. Using the notation given in Appendix 1 of Ref. [47], the HO radial functions $R_{nl}(\rho)$ are given by

$$R_{nl}(\rho) = (-1)^n \Big[\frac{2n!}{\Gamma(n+l+3/2)}\Big]^{\frac{1}{2}} \exp(\frac{-\rho^2}{2}) \rho^l L_n^{l+\frac{1}{2}}(\rho^2) \,, \tag{2.6}$$

where $L_n^{l+\frac{1}{2}}(x)$ are the generalized Laguerre polynomials, $\Gamma(z)$ is the Euler gamma function, the HO length $b = \sqrt{\frac{\hbar^2}{m_r \hbar\Omega}}$ with $m_r = \frac{1}{2}m$ being the reduced mass of the 2N system, the average nucleon mass $m = \frac{m_n + m_p}{2}$ and $\hbar\Omega = 40$ MeV.

Since momentum space matrix elements of the JISP16 potential are restricted to low momenta, we will compare its predictions to results obtained with a number of $V_{\text{low k}}$ potentials, whose nonzero matrix elements are restricted to momenta inside intervals of decreasing size, generated from the neutron-proton version of the high-precision CD Bonn interaction. To obtain the matrix elements of the $V_{\text{low k}}$ potential, we use the Ōkubo theory [48] of the unitary transformation which splits the Hilbert space into low and high momenta subspaces. Namely, in order to separate the momentum space to a low-momentum region and a high-momentum one, we introduce the following projection operators (P and Q)

$$\begin{aligned} P &= \int_0^\Lambda |p\rangle\langle p| dp, \\ Q &= \int_\Lambda^\infty |p\rangle\langle p| dp, \end{aligned} \tag{2.7}$$

where Λ is a momentum cutoff whose value will be specified later. Given the unitary transformation operator of the Ōkubo theory, the effective Hamiltonian $PH'P$ in the P space takes the form

$$PH'P = P(1+\omega^\dagger\omega)^{-\frac{1}{2}}(H + \omega^\dagger H + H\omega + \omega^\dagger H\omega)(1+\omega^\dagger\omega)^{-\frac{1}{2}}P, \tag{2.8}$$

where the original Hamiltonian H consists of the kinetic energy H_0 and the original potential V and where ω is a wave operator which satisfies the condition $\omega = Q\omega P$. Then the low-momentum potential $V_{\text{low k}}$ is obtained as

$$V_{\text{low k}} = PH'P - PH_0P. \tag{2.9}$$

	$E_{\rm deu}$ [MeV]	P($^3S_1$)	P($^3D_1$)	$\langle E_{\rm pot}\rangle$ [MeV]	$\langle E_{\rm kin}\rangle$ [MeV]
JISP16	−2.2246	96.02	3.98	−12.987	10.763
N^{4}LO (R=0.9 fm)	−2.2233	95.71	4.29	−21.115	18.892
AV18	−2.2422	94.22	5.78	−22.125	18.882
CD Bonn (non-rel)	−2.2232	95.14	4.86	−17.822	15.599

TABLE I. The deuteron g. s. energy $E_{\rm deu}$, the $^3S_1$ and $^3D_1$ state probabilities as well as the potential and the kinetic energy expectation values obtained with various NN interactions.

The details of the two methods to obtain the wave operator ω are given in Refs. [34, 49, 50], and in this paper we make use of the Suzuki Method II [49]. As will be discussed in Sec.V, the Λ cut-off value determines the range of incoming nucleon energy where such a $V_{\rm low\ k}$ potential is applicable. Even an extension of this method to the unitary transformation in the three-particle space and taking into account additional 3N interactions emerging from such a transformation, will not result in a proper description of 3N observables at relative initial momenta above the value given by the cut off parameter.

In the case of the chiral interaction, we use the N^{4}LO neutron-proton force [7, 8] with the semi-local regularization induced in coordinate space by the regulator function $f(r) = [1 - \exp(-(\frac{\rm r}{\rm R})^2)]^6$, with the regulator value R=0.9 fm.

III. THE BOUND STATES

The neutron-proton phase shifts obtained with the JISP16 force agree very well with values extracted from experimental data by the Nijmegen group [51] up to the nucleon laboratory energy 350 MeV. Below 200 MeV the only deviation, around 15%, is observed for the $^3S_1 - {}^3D_1$ mixing parameter ϵ_1 at energies lower than ≈ 40 MeV.

The deuteron properties are also very well reproduced by the JISP16 potential [52]. The deuteron ground state (g. s.) energy, which is one of the observables used to fix potential parameters, agrees with the experimental value $E_{\rm deu} = -2.22457$ MeV for the JISP16 as well as for other NN interaction models. In Tab. I we give a few additional quantities which are not observables but which shed some light on the deuteron properties arising from various forces. The $^3D_1$ state probability takes the smallest value for the JISP16 force but remains close to numbers obtained with the other models. The expectation values of the potential and kinetic energy in the deuteron for the JISP16 model differ significantly from the corresponding numbers obtained with other interactions. That difference can be understood after examining the deuteron wave functions given by these potentials, which are shown in Fig. 1, in coordinate ($\tilde{\psi}_{deu}(r)$) and momentum ($\psi_{deu}(p)$) spaces. The $^3S_1$ component of the JISP16 deuteron wave function in coordinate space decreases monotonically contrary to the $^3S_1$ wave functions for other NN interactions, which all have a maximum around $r = 1$ fm (see Fig. 1). All $^3D_1$ state wave functions have a maximum, which for the JISP16 is localized at $r \approx 2$ fm while for the other potentials at $r \approx 1$ fm. In momentum space both components of the deuteron wave function for the JISP16 interaction are compressed to smaller momenta compared to the other potential predictions. This is clearly seen also in the inset in the left column and the bottom row of Fig. 1. For the JISP16 force the $^3S_1$ $\psi_{deu}(p)$ drops quickly and becomes negligible above $p \approx 2.5$ fm^{-1}. The $^3S_1$ deuteron wave function for the other potentials shows a shallow minimum at these momenta and approaches zero at momenta

above p=5 fm^{-1}. The differences in the behavior of $^3S_1$ wave functions explain the energy expectation values, shown in Tab. I—the wave function localized at lower momenta (see lower panels of Fig. 1) leads to a smaller expectation value of the kinetic and thus also of the potential energy.

Predictions for the triton binding energy as well as for the kinetic and potential energy expectation values in the triton are presented in Tab. II. The ^{3}H g. s. energy obtained with the JISP16 interaction is much closer to the experimental value (−8.482 MeV [53]) than predictions based on the other NN forces. This is another example where the pairwise JISP16 model alone works well in nuclear structure calculations without resorting to additional 3N dynamics. For the other potentials listed in Tab. II one needs explicit 3NF's to explain the triton binding energy as exemplified for the AV18+Urbana IX combination. The expectation values of the kinetic energy and the two-body part of the potential energy operators in the triton show the same tendencies as in the deuteron case: again the values obtained by using the JISP16 force are significantly smaller than ones for the other models. Comparing the g. s. energies given in Tab. II with experimental values one has to be aware that the JISP16 model neglects charge independence breaking of the NN force. However one can think about the JISP16 force as about an effective interaction with parameters fixed by data from many-nucleon systems, which may include some effects of charge independence breaking. The effect of mimicking the charge dependence in many-body systems by off-shell properties of charge-independent NN interaction is more pronounced in another interaction fitted to many-nucleon systems, the Daejeon16 [54] which reproduces the binding energies

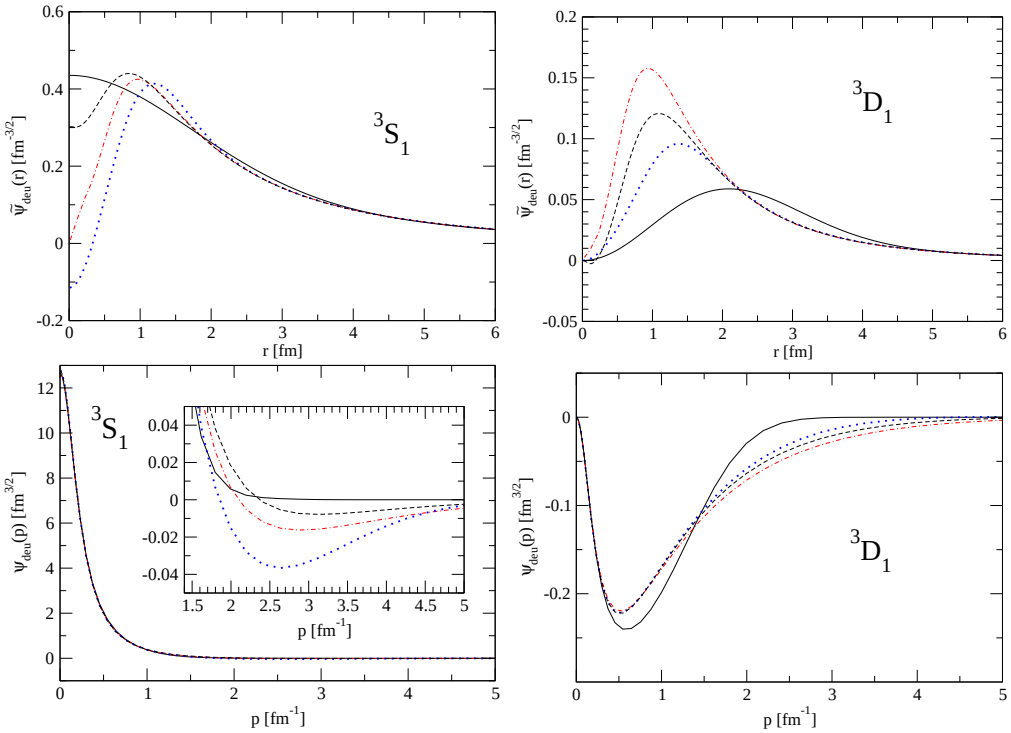

FIG. 1. (color online) The deuteron wave functions in coordinate $\tilde{\psi}_{deu}(r)$ (top) and momentum $\psi_{deu}(p)$ (bottom) space, respectively. The $^3S_1$ and the $^3D_1$ components are shown in the left and right columns, respectively. The black solid, red dash-dotted, black dashed and blue dotted curves are for the JISP16, the AV18, the CD Bonn and the chiral N^{4}LO forces, respectively.

	$E_{3\mathrm{H}}$ [MeV]	$\langle E_{\mathrm{pot}}^{(NN)} \rangle$ [MeV]	$\langle E_{\mathrm{pot}}^{(3N)} \rangle$ [MeV]	$\langle E_{\mathrm{kin}} \rangle$ [MeV]
JISP16	−8.369	−35.766	−	27.399
N^{4}LO ($R = 0.9$ fm)	−7.828	−56.952	−	49.124
AV18	−7.656	−54.461	−	46.805
AV18+Urbana IX	−8.507	−58.686	−1.123	51.304

TABLE II. The ^{3}H g. s. energy $E_{3\mathrm{H}}$ and the expectation values for the 2N potential energy ($E_{\mathrm{pot}}^{(NN)}$), the 3N potential energy ($E_{\mathrm{pot}}^{(3N)}$) and the kinetic energy (E_{kin}) obtained with various NN or NN+3N interactions.

of not only $N = Z$ nuclei but also of nuclei with large difference of numbers of neutrons and protons like, e.g. ^{10}He.

The possibility of avoiding explicit 3NF's when using the two-body JISP16 interaction for explaining nuclear binding energies prompted us to check if this strategy could be successful in Nd scattering. It would be an interesting finding, since up to now while using high precision, standard or chiral NN potentials, resorting to explicit 3NF's is mandatory at higher energies in order to explain data for some scattering observables.

IV. Nd SCATTERING WITH JISP16, SEMI-PHENOMENOLOGICAL AND CHIRAL FORCES

In this section we present predictions obtained with the JISP16, the semi-phenomenological and the chiral N^{4}LO NN forces for various observables in the Nd scattering process at incoming nucleon laboratory energies $E = 5$, 13, 65 and 135 MeV. Since the JISP16 potential has been derived only for the neutron-proton system, we use also the neutron-proton version of the corresponding NN interaction in calculations with other forces. In some of the following figures we compare our predictions also to the proton-deuteron data, what is justified by small effects of the Coulomb force (neglected in the theoretical calculations). Such effects are only visible at lower energies and forward scattering angles [55].

Differential cross sections at the above listed energies are shown in Fig. 2. At $E = 5$ MeV the predictions based on the JISP16 cross section (black solid curve) practically do not differ from those for the AV18 (the red dashed curve) or the chiral N^{4}LO (the blue dash-dotted curve) forces. They are also very close to the predictions based on the AV18 NN potential combined with the Urbana IX 3N force indicating that at this energy 3NF effects are practically negligible for the elastic scattering cross section. This picture changes at higher energies. At $E = 13$ MeV in the region around the minimum of the cross section the JISP16 predictions are approximately 10% below the other practically overlaping predictions. Since also here the AV18 and AV18+Urbana IX results are nearly the same, we conclude that 3NF effects in the elastic scattering cross section are negligible for this energy, too. At $E = 65$ MeV the JISP16 predictions in the same region of angles are approximately 15% above the data. Here AV18+Urbana IX prediction describes the data well while the results of the other two NN potentials overlap and clearly underestimate the experimental values. At this and at higher energies the 3NF plays an important role in the region around the minimum of the cross section—the AV18 predictions are substantially increased by taking the Urbana IX force into account. The JISP16 predictions are, when compared to the other NN based results, shifted in the same direction as AV18+Urbana IX predictions, however

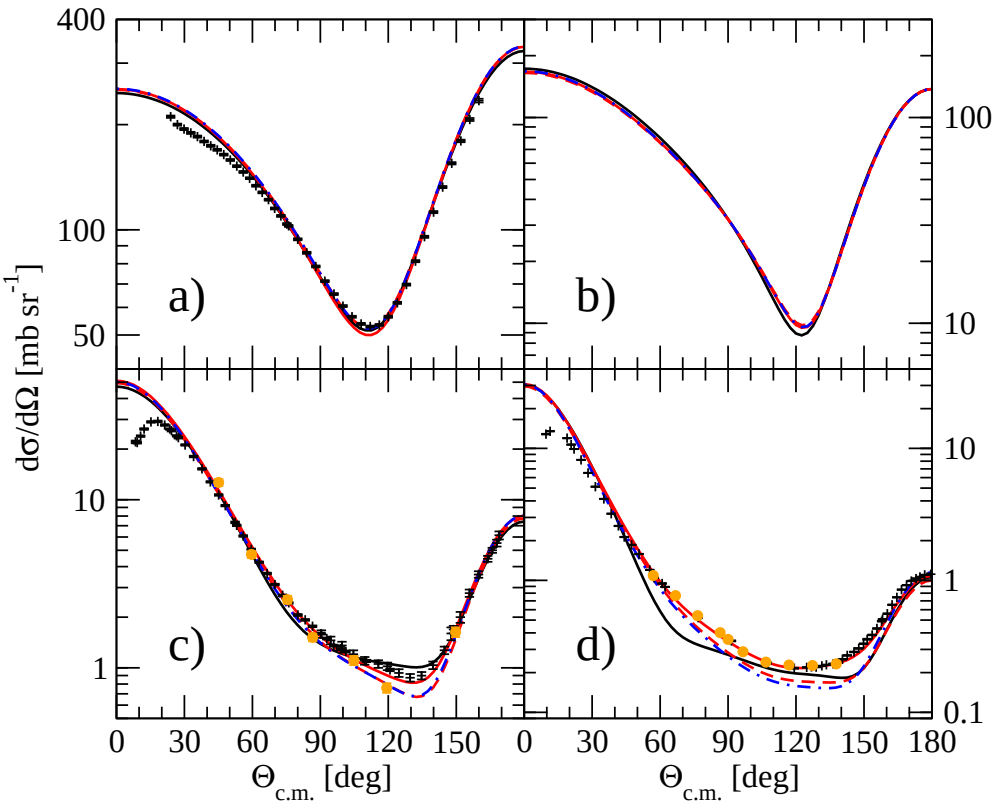

FIG. 2. (color online) The differential cross section dσ/dΩ [mb sr^{-1}] for elastic Nd scattering at the incoming nucleon laboratory energy a) $E = 5$ MeV, b) $E = 13$ MeV, c) $E = 65$ MeV and d) $E = 135$ MeV as a function of the center-of-mass scattering angle $\theta_{\rm c.m.}$. The black solid, red dashed, red solid and blue dash-dotted curves represent predictions based on the JISP16, AV18, AV18+Urbana IX and chiral N^{4}LO (with the regularization parameter $R = 0.9$ fm) forces, respectively. The data are in a) from Ref. [56] (*pd* pluses), in c) from Ref. [57] (*pd* pluses) and [58] (*nd* orange circles) and in d) from Ref. [59] (*pd* pluses) and [60] (*pd* orange circles).

this shift is too strong and results in overestimating the data. At $E = 135$ MeV the deviation of the JISP16 predictions from the others increases significantly. While in the minimum of the cross section the JISP16 results are closer to the data than those for the AV18 and the chiral forces, at scattering angles $\theta_{\rm c.m.}$ in the range between 50° and 80° one observes a serious discrepancy from the data and from the other predictions. It is interesting to note that at this energy all cross section predictions overlap up to $\theta_{c.m.} \approx 50°$.

Fig. 3 presents the deuteron vector analyzing power iT$_{11}$ as a representative for vector analyzing powers. Contrary to the cross section, the iT$_{11}$ is the observable for which the JISP16 model fails completely even at the lowest energy. The predictions based on the JISP16 force at $E = 5$ MeV and $E = 13$ MeV, are about twice as large as predictions obtained with the other interactions. Despite the big difference in the magnitudes, the shapes of the iT$_{11}$ curves are similar. At $E = 65$ MeV the JISP16 predictions come closest to those of the other interactions, which agree well with the data, while diverging from them around the minimum of the analyzing power and around $\theta_{\rm c.m.} = 145°$. It is interesting to note that up to $\theta_{c.m.} \approx 80°$ the JISP16 provides practically the same predictions as the other forces, giving a good description of data at this energy. Only above that angle

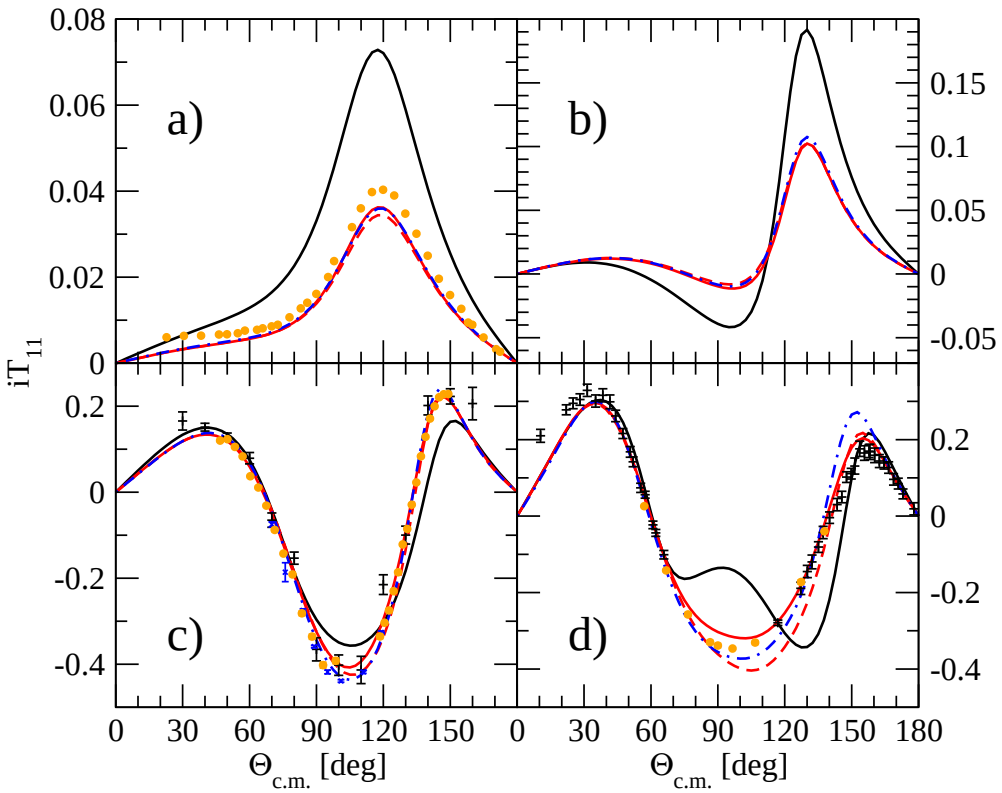

FIG. 3. (color online) The deuteron analyzing power iT_{11} for elastic Nd scattering at the incoming nucleon laboratory energy a) E=5 MeV, b) E=13 MeV, c) E=65 MeV and d) E=135 MeV as a function of the center-of-mass scattering angle $\theta_{\rm c.m.}$. Curves are as in Fig. 2. The data in a) are from Ref. [61] (*pd* orange circles), in c) are from Ref. [62] (*pd* pluses), [63] (*pd* orange circles) and [64] (*pd* blue x-es), and in d) from Ref. [59] (*pd* pluses) and [60] (*pd* orange circles).

the deviations from the other predictions (and data) start to develop. At $E = 135$ MeV the JISP16 predictions follow the data at scattering angles below $\theta_{\rm c.m.} = 70°$ and above $\theta_{\rm c.m.} = 150°$, missing the data and other predictions at intermediate angles. At three lower energies the 3NF effects are negligible and the AV18, the AV18+Urbana IX, and N^{4}LO predictions agree with one another. At $E = 135$ MeV the observed 3NF effects are much smaller than the difference between the JISP16 and the AV18 or the chiral results.

The tensor analyzing power T_{22}, presented in Fig. 4, again shown as a representative of observables arising from tensor polarization states, belongs to the class of observables that have been proven, at higher energies, to be sensitive to fine details of the interaction model. Predictions based on the JISP16 potential start to deviate slightly from the others already at $E = 13$ MeV but at $E = 65$ MeV this deviation becomes large, resulting in a major disagreement with the data above $\theta_{c.m.} \approx 30°$. At $E = 135$ MeV the JISP16 interaction is not able to describe the data, showing an unexpected maximum at $\theta_{\rm c.m.} = 95°$. At the two higher energies 3NF effects are clearly visible, however supplementing the AV18 interaction with the Urbana IX 3NF moves predictions at $E = 135$ MeV farther away from the data. Even on the level of two-body interactions the difference between the AV18 and the N^{4}LO predictions is large for scattering angles around 130° and the AV18 results provide the best description of the data.

Summarizing above results as well as results for remaining, not shown here, elastic scat-

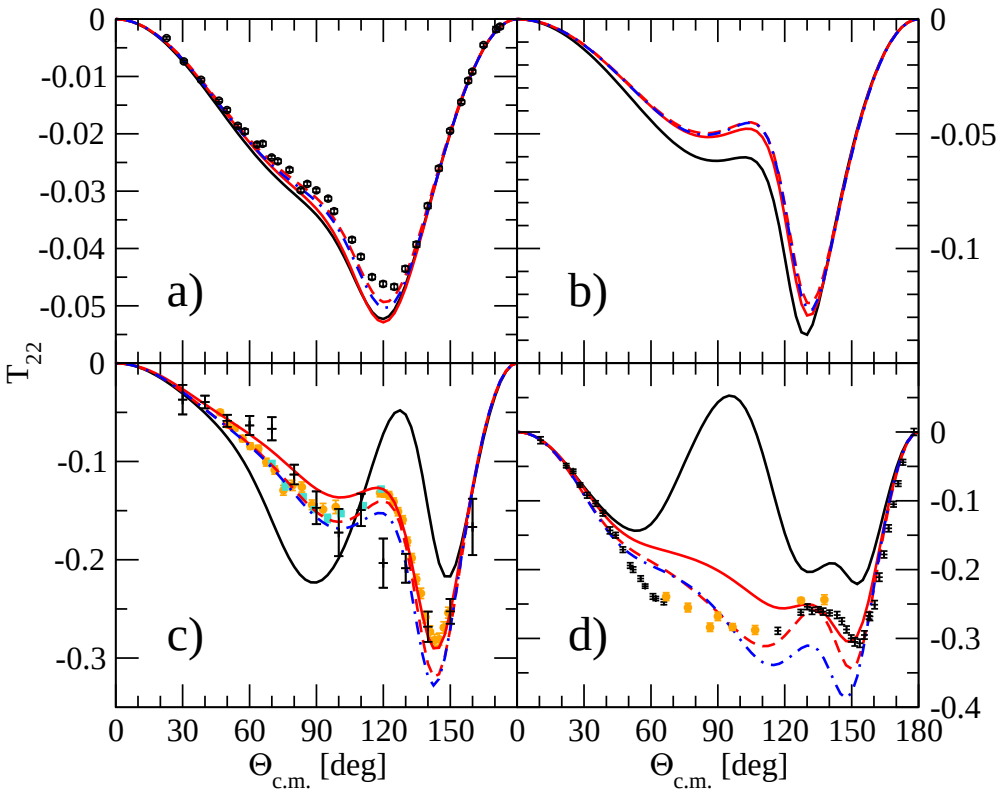

FIG. 4. (color online) The deuteron tensor analyzing power T_{22} for elastic Nd scattering at the incoming nucleon laboratory energy a) $E = 5$ MeV, b) $E = 13$ MeV, c) $E = 65$ MeV and d) $E = 135$ MeV as a function of the center-of-mass scattering angle $\theta_{\rm c.m.}$. Curves are as in Fig. 2. The data in a) are from Ref. [61] (*pd* circles), in c) are from Ref. [62] (*pd* pluses), [63] (*pd* orange circles) and [64] (*pd* turquoise squares), and in d) are from Ref. [59] (*pd* pluses) and [60] (*pd* orange circles).

tering observables, we can state that the modern nuclear forces, including the JISP16 model, have problems with a precise description of many polarization observables. Moreover, we conclude that the predictions of the Nd elastic scattering observables obtained with the JISP16 force are not closer to results arising from the AV18 plus Urbana IX interactions than to the results obtained when using only NN forces. In addition, the JISP16 model predictions miss the data in broad ranges of the scattering angles. This is seen very clearly at higher energies, but for some observables also at the relatively small energy of 5 MeV.

Thus the question arises: what is the reason for such a behavior? We already noticed that the JISP16 deuteron wave function is shifted towards lower momenta compared with the wave functions calculated using the other interaction models. Since the deuteron wave function is an important ingredient of elastic Nd scattering, it is worth investigating if the (shifted to small momenta) deuteron wave function can be linked with the observed discrepancies. To this end we performed calculations with the chiral N^{4}LO semi-locally regularized interaction (with the regulator $R = 0.9$ fm) but to calculate observables we replaced the chiral N^{4}LO deuteron wave function by the one obtained from the JISP16 model. When calculating the chiral t-matrix the correct chiral wave function was used to determine the residue of the $^3S_1 - ^3D_1$ t-matrix. Having in mind a small deviation of the

mixing parameter ϵ in the ${}^3S_1 - {}^3D_1$ partial wave we also repeated calculations with the JISP16, but used the chiral t-matrix in that coupled channel instead of the original JISP16 t-matrix. Again, the correct residue of the ${}^3S_1 - {}^3D_1$ t-matrix, given by the chiral deuteron wave function was used. Results at $E = 5$ MeV are shown in panel a) of Fig. 5. We focus there on the analyzing power iT_{11}, for which the discrepancy between the JISP16 predictions and those of the chiral interaction is very pronounced. As is seen in Fig. 5a) the iT_{11} practically does not change when the JISP16 deuteron wave function is used together with the chiral NN force (magenta dotted vs blue dash-dotted curves). Also there is only a tiny effect due to changing the ${}^3S_1 - {}^3D_1$ t-matrix (black solid vs red dashed curves). Analyzing the importance of the remaining partial waves for this observable we found, that the interference of different P-waves is responsible for the observed difference between the JISP16 and chiral predictions. This is documented in the middle and in the right panels of Fig. 5. Namely, in the middle panel we show what happens if only a single partial wave (channel) component is replaced in the t-matrix. While exchanging most of channels has only a small effect on the iT_{11}, exchanging separately ${}^3P_0$, ${}^1P_1$, or ${}^3P_2 - {}^3F_2$ waves leads to a significant change in the iT_{11} magnitude (see dashed black, solid green and solid magenta curves respectively). However, it is clear, that none of these waves is able alone to explain the difference between the JISP16 and the chiral N^{4}LO predictions. The right panel in Fig. 5 shows effects of exchanging two or three partial waves at the same time. We see that the simultaneous exchange of the lowest P-waves: ${}^3P_0$, ${}^1P_1$ and ${}^3P_2 - {}^3F_2$ shifts predictions close to the N^{4}LO results. We conclude, that an interplay of these partial waves during solving Eq. (2.3) enhances reduction of the iT_{11} values. Of course, the deuteron vector analyzing power at low energies is known to be sensitive to the P-waves but results shown in Fig. 5 clearly indicate that the strength of the P-waves components of the JISP16 interaction should be corrected.

The observation drawn from Fig. 5 is also true for the remaining observables at the low energies: the replacement of the P-waves components from the JISP16 potential by the corresponding ones generated by the N^{4}LO interaction moves the JISP16 based predictions into the vicinity of the complete chiral N^{4}LO results.

The picture becomes more complex at the higher energies, where the importance of higher partial waves grows. The simultaneous replacement of only the ${}^1P_1$, ${}^3P_0$ and ${}^3P_2 - {}^3F_2$ JISP16 t-matrix elements by those from the N^{4}LO is insufficient to move predictions to the vicinity of the complete chiral results. In Fig. 6 we show the differential cross section, the deuteron vector analyzing power iT_{11} and the deuteron tensor analyzing power T_{22} at $E = 65$ MeV as examples of this different behavior under the change of the selected partial wave components of the t-matrix. The range of scattering angles presented in Fig. 6 is restricted to the regions where the differences between various predictions are most noticeable.

The left panel of Fig. 6 shows the minimum of the differential cross section. The change of the P-waves (black dotted curve) has only a small influence on the magnitude of the cross section. A subsequent replacement of all t-matrix components up to the two-body total angular momentum $j \leq 2$ (the dashed magenta curve) moves predictions in the direction of the N^{4}LO results but this process stops with an increasing number of replaced partial wave components, as is visible from the cyan solid curve, which shows results with all t-matrix partial components exchanged up to $j \leq 3$. The deuteron wave function and its propagation in the solution of the Faddeev equation can explain most of the remaining differences between predictions with the substituted partial wave components and complete N^{4}LO results. Namely, we show also (by green double-dot-dashed curve) the results obtained

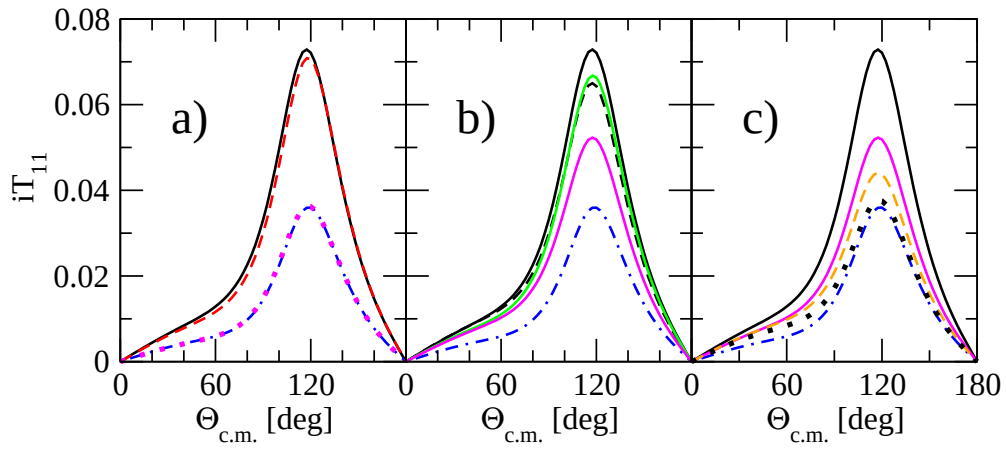

FIG. 5. (color online) The deuteron analyzing power iT_{11} at the incoming nucleon laboratory energy $E = 5$ MeV obtained with different inputs to Eq. (2.3). In all panels the black solid and blue dash-dotted curves are the same as in Fig. 3 and represent the JISP16 and chiral N^{4}LO predictions, respectively. In a) the magenta dotted curve shows results obtained with the chiral N^{4}LO force but using the JISP16 deuteron wave function. The predictions obtained with the JISP16 force with exception of $^3S_1 - {}^3D_1$ t-matrix components which were replaced by the chiral N^{4}LO ones are shown by a red dashed curve. In panel b) the green solid, black dashed and magenta solid curves represent JISP16 calculations with the exchanged t-matrix components in the $^1P_1$, $^3P_0$ and $^3P_2 - {}^3F_2$ channels, respectively. Finally, in panel c) different combinations of the t-matrix partial wave components are exchanged: $^3P_2 - {}^3F_2$ [the solid magenta curve, the same as in b)], $^3P_0$ and $^3P_2 - {}^3F_2$ (the dashed orange curve) and $^1P_1$, $^3P_0$ and $^3P_2 - {}^3F_2$ (the dotted black curve).

with the chiral N^{4}LO t-matrix combined with the deuteron wave function from the JISP16 force, which are reasonably close to the cyan solid curve. For the deuteron vector analyzing power, shown in the middle panel, the exchange of only the lowest P-wave components does not affect the predictions substantially. Only the change of the t-matrix in all partial wave components with $j \leq 2$ moves predictions close to the chiral results. Substituting the higher partial wave components does not change results significantly. The remaining differences are due to the different deuteron wave functions and are visible near the minimum of the iT_{11}. In the case of the deuteron tensor analyzing power T_{22} (the right panel) the same modification of all the partial wave components with $j \leq 2$ does not reproduce the chiral results either. While the maximum of the T_{22} observed for the JISP16 force around the scattering angle $\theta_{c.m.} = 130^\circ$ is substantially reduced, the emerging minimum of the T_{22} at the scattering angles $140^\circ \leq \theta_{c.m.} \leq 150^\circ$ is clearly too deep. Moreover, even the replacement of the higher partial wave components (up to $j \leq 3$) does not remedy this situation. Again the role of the deuteron wave function is important.

Finally, we would like to comment briefly on the behaviour of the JISP16 force in the deuteron-breakup reaction. In general, the picture obtained with the JISP16 interaction for the deuteron breakup resembles the one for the elastic scattering. Beside the kinematical configurations in which predictions for the exclusive cross section based on the JISP16 force are in quantitative agreement with predictions of other interactions even at higher energies, there are configurations in which the JISP16's results clearly differ from remaining predictions. What is interesting, one of such configurations is the SST configuration [44], for which cross section is known to be only slightly sensitive to the choice of the NN interaction.

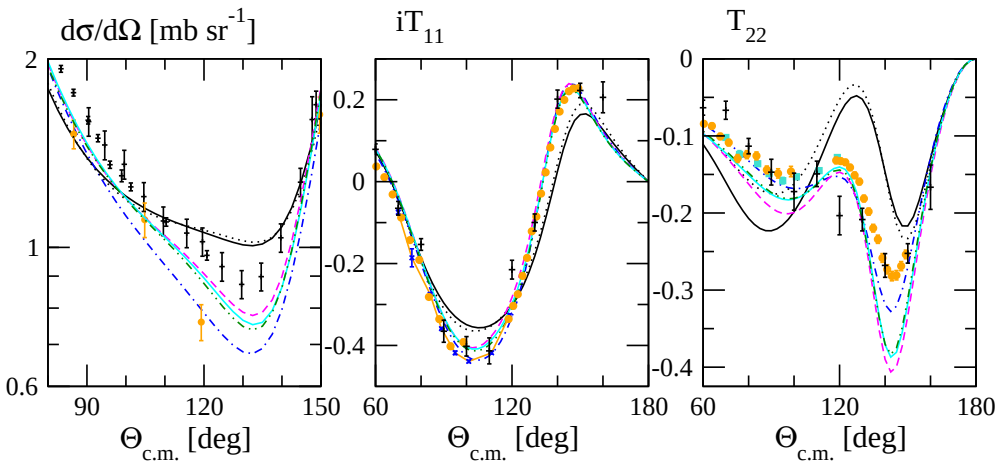

FIG. 6. (color online) The differential cross section (left panel), the deuteron analyzing power iT_{11} (the middle panel) and the deuteron tensor analyzing power T_{22} at the incoming nucleon laboratory energy $E = 65$ MeV obtained with different inputs to Eq. (2.3). In all panels the black solid and blue dash-dotted curves are the same as in Figs. 2- 4 and represent the JISP16 and chiral N^{4}LO predictions. In addition, there are three curves representing predictions obtained with the JISP16 force but replacing selected sets of the t-matrix partial wave components with those taken from the chiral N^{4}LO potential: $^1P_1$, $^3P_0$ and $^3P_2 - {}^3F_2$ (black dotted), all partial waves with $j \leq 2$ (magenta dashed) and all partial waves with $j \leq 3$ (cyan solid). Finally, the green dash-double-dotted curve shows predictions with the chiral N^{4}LO potential but with the deuteron wave function generated by the JISP16 NN force. The displayed data follow Figs. 2, 3 and 4 for the cross section, the iT_{11} and the T_{22}, respectively.

In Fig.7 we show the exclusive SST differential cross section $d^5\sigma/d\Omega_1\Omega_2 dS$ at energies used above for the elastic scattering. The JISP16 predictions differ from those obtained with the other NN interactions: at E=5 and E=13 MeV the differential cross section based on the JISP16 force is below other predictions obtained with two-body forces (approx. by 7% and 4% in the centre of plateau at E=5 MeV and E=13 MeV, respectively) while at higher energies it exceeds other results (approx. by 15% and 18% in the centre of plateau at E=65 MeV and E=135 MeV, respectively). At E=5 MeV the JISP16 predictions are close to ones for the AV18+UrbanaIX model what can reflect the incorporation of 3NF effects into the JISP16 interaction. Also at higher energies results with the JISP16 are shifted, compared to the other NN predictions, in the same direction as the AV18 + Urbana IX results. However, at the two higher energies this shift is too strong. Such a picture of the JISP16 SST cross section behaviour is one more hint that this force requires a careful revision as already have been concluded from our analysis of the Nd elastic scattering.

We can summarize our findings to this stage by a) pointing to the necessity of improvement of the P-wave components in the JISP16 NN potential model and b) asking a more general question about usefulness of soft potentials in a description of nuclear reactions at intermediate energies. In the next section we explore the latter issue by studying Nd scattering with a $V_{\rm low\,k}$ potential.

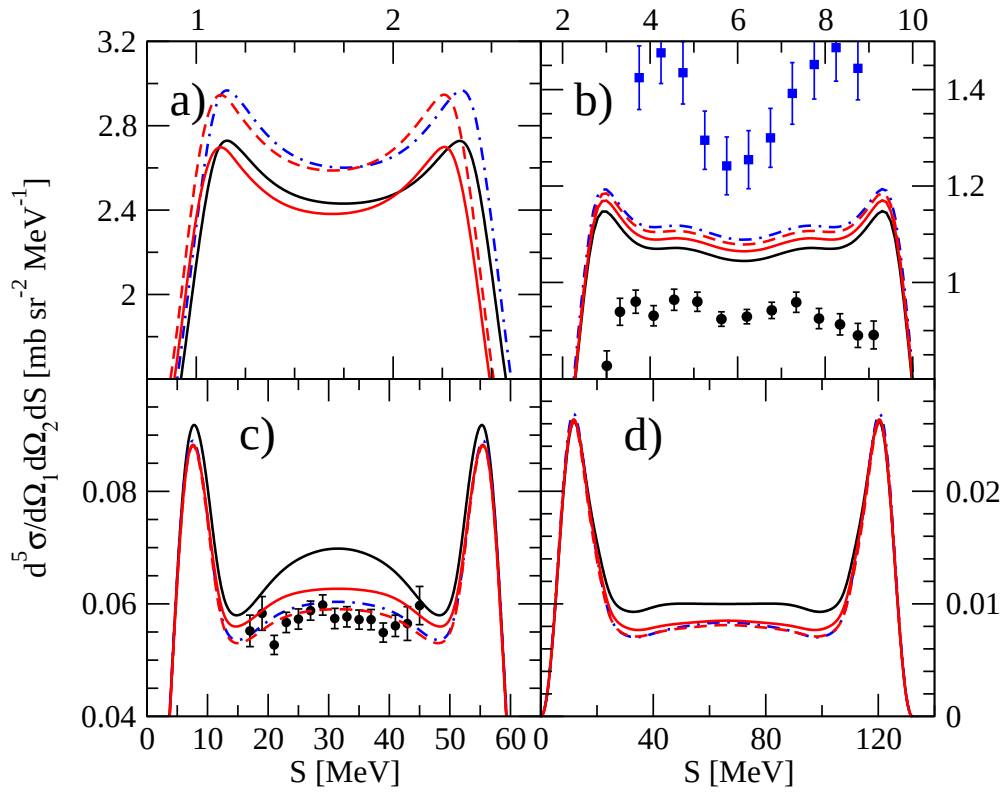

FIG. 7. (color online) The differential cross section $d^5\sigma/d\Omega_1\Omega_2 dS$ for the SST configuration in the deuteron breakup process at the incoming nucleon laboratory energy a) E=5 MeV, b) E=13 MeV, c) E=65 MeV and d) E=135 MeV as a function of the arc length S of the S-curve [44]. The polar angles of momenta of two measured neutrons are $\Theta_1 = \Theta_2 = 39.2°$ at E=5 MeV, $\Theta_1 = \Theta_2 = 50.5°$ at E=13 MeV, $\Theta_1 = \Theta_2 = 54.0°$ at E=65 MeV and $\Theta_1 = \Theta_2 = 54.4°$ at E=135 MeV, while the relative azimuthal angle $\Phi_{1-2} = 120°$ at all energies. Curves are as in Fig. 2. The data in b) are from Refs. [65, 66] (*nd* blue squares) and from Ref. [67] (*pd* black circles), and in c) are from Ref. [68] (*pd* circles).

V. Nd SCATTERING — JISP16 AND LOW MOMENTUM POTENTIALS

In the following we check whether softening the potential, of course within reasonable limits, could lead to problems with a description of Nd scattering observables. If it is possible to construct a NN potential whose matrix elements in momentum space can be restricted to low momenta and which at the same time guarantees a good description of observables in few-nucleon reactions, such a force would have very welcome properties from the point of view of nuclear structure calculations and lead to reduced computational costs. Thus in this section we compare predictions obtained with the CD Bonn and the JISP16 NN potentials to ones based on the $V_{\rm low\,k}$ potential derived from the CD Bonn force. We use the cutoff values $\Lambda = 1.0$ (for the deuteron bound state only), 1.5, 2.0 and 5.0 fm^{-1}.

The corresponding deuteron wave functions are shown in Fig. 8. At the largest value of Λ=5 fm^{-1} the two components, $^3S_1$ and $^3D_1$, of the deuteron wave function obtained with this $V_{\rm low\,k}$ force are very close to the original CD Bonn results. They both have a characteristic maximum in coordinate space at $r = 1$ fm. Changing Λ to smaller values,

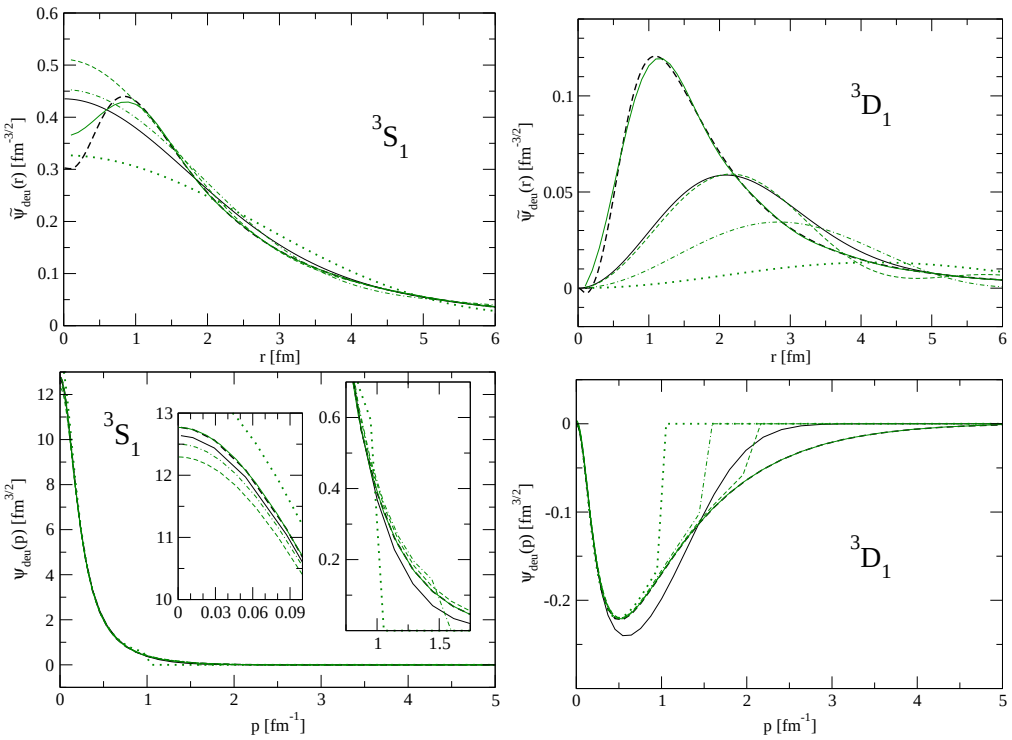

FIG. 8. (color online) The deuteron wave functions $\tilde{\psi}_{deu}(r)$ (top) and $\psi_{deu}(p)$ (bottom) in coordinate and momentum space, respectively. The $^3S_1$ and the $^3D_1$ components are shown in the left and the right column, respectively. The black solid and the black dashed curves represent the JISP16 and the CD Bonn predictions. The green dotted, dash-dotted, dashed and solid curves show wave functions obtained with the $V_{\rm low\,k}$ interaction based on the CD Bonn force, with cutoff values $\Lambda = 1.0$, 1.5, 2.0 and 5.0 fm^{-1}, respectively.

the $^3S_1$ wave function in coordinate space loses that maximum and monotonically decreases with r, similarly to the JISP16 coordinate space $^3S_1$ deuteron component. In momentum space, the same convergence pattern with Λ is seen and in addition a clear limitation of nonzero wave function components to momenta below Λ is observed. The probability values for both components of the deuteron wave function together with the expectation values of kinetic and potential energies are given in Tab. III.

The JISP16 interaction is designed as a matrix in the oscillator basis covering the NN relative motion up to momenta of approximately 2 fm^{-1}. Therefore it is not surprising that the JISP16 NN interaction has much in common with the $V_{\rm low\,k}$ forces, and indeed the JISP16 deuteron wave function is seen in Fig. 8 to be close to that from the $V_{\rm low\,k}$ potential with $\Lambda = 2$ fm^{-1}. Note however that the kinetic and potential energy expectation values in the deuteron given in Tab. III indicate that some features of the JISP16 are closer to those of the $V_{\rm low\,k}$ with $\Lambda = 1.5$ fm^{-1}.

Before we present our 3N scattering results, let us emphasize that the procedure that we apply to soften the CD Bonn potential and to construct the low momenta $V_{\rm low\,k}$ NN forces (i.e by applying unitary transformations with different values of the cutoff parameter Λ) preserves the good description of the NN system given by the CD Bonn potential. This is exemplified by the equal values of the deuteron g. s. energy $E_{\rm deu}$ given in Tab. III for the CD Bonn and different versions of $V_{\rm low\,k}$. However, that procedure, when applied to

a 3N system generates additional 3N forces [38, 39], which, generally speaking, should be included when performing 3N calculations. Neglecting those additional 3NF's can lead to misleading conclusions, with the exception of cases when the 3NF effects are negligible. From an approximate equality of the triton binding energies of the CD Bonn and $V_{\rm low\,k}$ NN force with Λ=5 fm^{-1} (see Tab. IV) it follows, that the effects of missing 3N forces are practically negligible for that observable at Λ=5 fm^{-1}. However, decreasing the cutoff Λ to Λ=2 fm^{-1} and Λ=1.5 fm^{-1}, makes the additional 3N interaction indispensable, since the $V_{\rm low\,k}$ predictions for the triton binding energy are significantly higher (by ≈ 0.7 MeV) than the CD Bonn results. Including the induced 3N force into the triton calculations should regain the CD Bonn result as was shown in Ref. [38] for the case of the chiral N^{3}LO potential and a number of low momenta forces generated from that interaction.

For the 3N scattering observables we give again a set of figures (Figs. 9–11) showing the differential cross section and the vector and tensor analyzing powers at the nucleon laboratory energies $E = 5$, 13, 65 and 135 MeV. Apart from the predictions obtained with the $V_{\rm low\,k}$ potential derived from the CD Bonn NN interaction for various values of the cutoff parameter Λ, we show the reference results based on the CD Bonn force, which corresponds to the limit $\Lambda \to \infty$. For the convenience of the reader we present again also the JISP16 predictions.

At the three lower energies $5, 13$, and 65 MeV the differential cross section, shown in Fig. 9, is stable with respect to changing the Λ value and cross sections for different cutoffs are close to the CD Bonn prediction. At $E = 135$ MeV only the predictions for Λ=1.5 fm^{-1} deviate drastically from the other cutoffs, which are close to the CD Bonn cross sections. The $\Lambda = 1.5$ fm^{-1} cross sections show strong variations with the scattering angle, which cannot be attributed to effects due to action of some 3NF, since such effects generally change smoothly with the scattering angle. It indicates that as far as the cross section is concerned the effects of the additional 3N force are at most moderate. Further we argue that the observed behavior of the cross section at 135 MeV and $\Lambda = 1.5$ fm^{-1} is dominated by kinematical restrictions coming into effect for low momenta interactions.

For polarization observables the picture is similar to the one for the cross section although they become somewhat more sensitive to variations of the cutoff parameter at some energies and angles (see Figs. 10 and 11 for representatives of the analyzing powers: iT_{11} and T_{22}). At the two lowest energies, $E = 5$ MeV and $E = 13$ MeV, predictions for the iT_{11} and T_{22} as well as for remaining, not shown here, polarization observables are practically insensitive to changes of the cutoff parameter. At these two energies results for all cutoffs are very

	$E_{\rm deu}$ [MeV]	P($^3S_1$)	P($^3D_1$)	$\langle E_{\rm pot}\rangle$ [MeV]	$\langle E_{\rm kin}\rangle$ [MeV]
JISP16	−2.225	96.02	3.98	−12.99	10.76
CD Bonn (non-rel)	−2.223	95.14	4.86	−17.82	15.60
$V_{\rm low\,k}$ with Λ=5.0 fm^{-1}	−2.223	95.17	4.83	−17.53	15.31
$V_{\rm low\,k}$ with Λ=2.0 fm^{-1}	−2.223	96.65	3.55	−14.22	12.00
$V_{\rm low\,k}$ with Λ=1.5 fm^{-1}	−2.223	97.48	2.52	−12.90	10.68
$V_{\rm low\,k}$ with Λ=1.0 fm^{-1}	−2.223	98.79	1.21	−11.13	8.81

TABLE III. The deuteron g. s. energy $E_{\rm deu}$, the $^3S_1$ and $^3D_1$ state probabilities as well as the potential and the kinetic energy expectation values obtained with different NN potentials: JISP16, CD Bonn and $V_{\rm low\,k}$ derived from the CD Bonn force.

	E_{3H} [MeV]	$\langle E_{pot}^{(NN)} \rangle$ [MeV]	$\langle E_{kin} \rangle$ [MeV]
JISP16	−8.37	−35.77	27.40
$V_{low\ k}$ with Λ=1.5 fm^{-1}	−8.97	−37.82	28.85
$V_{low\ k}$ with Λ=2.0 fm^{-1}	−8.84	−40.31	31.47
$V_{low\ k}$ with Λ=5.0 fm^{-1}	−8.27	−45.59	37.32
CD Bonn	−8.25	−46.40	38.15

TABLE IV. The ^{3}H binding energy E_{3H} and the expectation values for the 2N potential energy ($E_{pot}^{(NN)}$) and the kinetic energy (E_{kin}), obtained with various NN interactions only (taken as a neutron-proton force).

close to each other and to the CD Bonn potential prediction in the whole angular region. The same is true at $E = 65$ MeV for the iT_{11} for all Λ values. At that energy the tensor analyzing power T_{22}, shows only weak dependence on the cutoff value Λ (see Figs. 10 and 11). Overall, this indicates that, for polarization observables, the effects of the additional 3N forces are negligible, at least at the two largest Λ values.

Going to $E = 135$ MeV one finds again a picture similar to the one observed for the cross section at that energy. Again for both polarization observables the prediction with the smallest cutoff $\Lambda = 1.5$ fm^{-1} becomes drastically different from the others for angles above

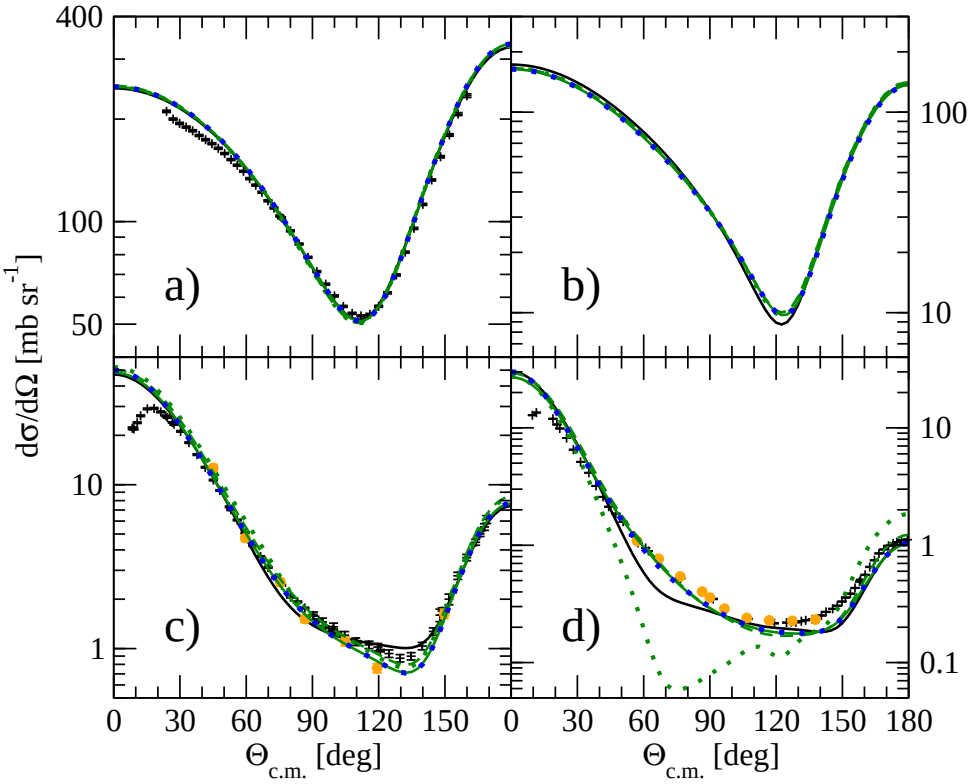

FIG. 9. (color online) The same as in Fig. 2 but for the theoretical predictions based on the $V_{low\ k}$ interaction with the cutoff parameters $\Lambda = 5$ fm^{-1} (the green solid curve), $\Lambda = 2$ fm^{-1} (the green dashed curve) and $\Lambda = 1.5$ fm^{-1} (the green dotted curve). The black solid curve represents the JISP16 predictions and is the same as in Fig. 2. The blue dotted curve is for the CD Bonn based results and overlaps with the green solid one.

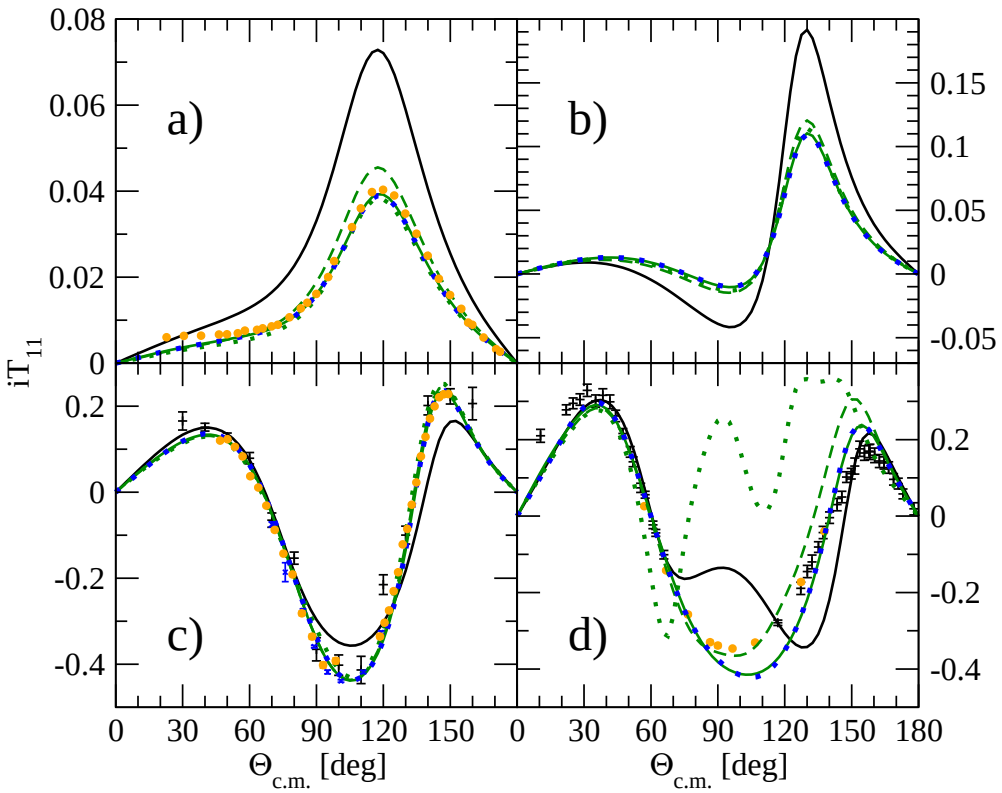

FIG. 10. (color online) The same as in Fig. 3 but for the theoretical predictions based on the $V_{\rm low\ k}$ interaction. Curves are as in Fig. 9 and data are as in Fig. 3.

some specific value, showing rapid angular variations. At this energy even predictions for $\Lambda = 2$ fm^{-1} start to reveal such a behavior which, like the behavior of the cross section at that energy, arises mostly from kinematical restrictions.

It is worth emphasizing that for all observables predictions based on the $\Lambda = 5$ fm^{-1} are at all four energies indistinguishable from the original CD Bonn results.

To explain the reason for such a behavior of the low momenta potential predictions let us stress that when using such interactions in 3N continuum calculations, a natural limitation appears and results obtained with such forces can be applied to interpret elastic Nd scattering data only up to a certain initial relative nucleon-deuteron momentum. That limitation follows from the fact that the momentum space deuteron wave function components as well as the momentum space matrix elements of such a low momentum $V_{\rm low\ k}$ potential are restricted to momentum values below the cutoff parameter Λ of that force. It means that application of such forces to interpret elastic Nd scattering data at specific incoming nucleon laboratory energy is possible only in a limited region of c. m. angles where the momentum transfer $\Delta q = 2q_0 \sin\frac{\theta_{c.m.}}{2}$ is smaller that Λ. (Here q_0 is the magnitude of the relative nucleon-deuteron momentum.) It restricts the application of low momentum potentials to the c. m. angles below $\theta^{lim}_{c.m.} = 2\arcsin(\frac{\Lambda}{2q_0})$ for a given incoming nucleon energy and thus also restricts the incoming nucleon laboratory energy to a region below $E^{lim}_{lab} = \frac{9}{32m}\Lambda^2$ (m is the nucleon mass), where predictions should be valid over the whole angular range. In Tab. V we show that limiting angle at each energy studied in the present paper for two values of $\Lambda = 1.5$ fm^{-1} and $\Lambda = 2$ fm^{-1}. Assuming that effects of additional 3N forces are

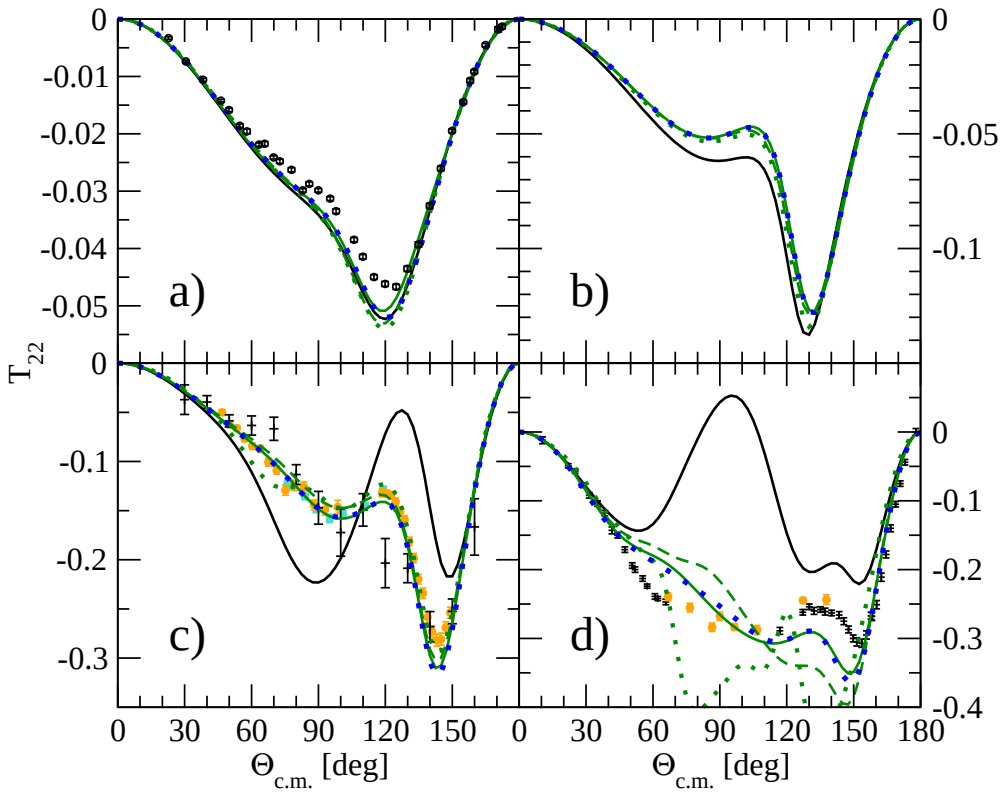

FIG. 11. (color online) The same as in Fig. 4 but for the theoretical predictions based on the $V_{\rm low\ k}$ interaction. Curves are as in Fig. 9 and data are as in Fig. 4.

negligible, as we inferred for certain kinematic regions from the above analysis and what in addition is supported by results of Ref. [40], it follows from the numbers given in Tab. V, that the low momentum interactions $V_{\rm low\ k}$ should provide an equally good description of Nd elastic scattering data as the CD Bonn potential at the two lowest energies $E = 5$ MeV and $E = 13$ MeV. The deviations from the CD Bonn potential based predictions can appear at $E = 65$ MeV and $E = 135$ MeV, where the limiting angle restricts description to angles below $\theta^{lim}_{c.m.}$. At these energies, especially for $E = 135$ MeV and $\Lambda = 1.5$ fm^{-1}, where the limiting angle is smallest, for some observables low momentum interaction predictions follow the CD Bonn ones only for angles up to $\approx \theta^{lim}_{c.m.}$, diverging strongly at the larger angles. This is just what is seen in Figs. 9–11. Since the JISP16 behaves in some respects similarly to the low momentum $V_{\rm low\ k}$ potential for $\Lambda = 2$ fm^{-1}, the above arguments explain also the behavior of its predictions seen in Figs. 9–11. One could argue that in order to get a proper description of data by such a low momentum interaction in the whole angular range, the following restriction on the momentum transfer should be imposed: $2q_0 \leq \Lambda$. This in turn can be used to establish the maximal energy, below which low momentum potentials can be applied to interpret the full angular range of the Nd elastic scattering data, E^{lim}_{lab}. That restriction gives for $\Lambda = 2$ fm^{-1} the limiting energy of $E^{lim}_{lab} = 46.7$ MeV and the limiting energy of $E^{lim}_{lab} = 26.2$ MeV for $\Lambda = 1.5$ fm^{-1}. These conclusions are further supported by the (not shown here) results obtained with the cutoff value $\Lambda = 3.5$ fm^{-1} at $E = 135$ MeV (at this energy $2q_0 = 2 * 1.70$ fm^{-1}=3.4 fm^{-1}) for which we observe a good agreement between $V_{\rm low\ k}$ and CD Bonn predictions over the full angular range for all observables. Thus in any future attempts to improve the JISP16 potential by adjusting its parameters to the elastic

scattering Nd data in addition to NN and many-body nuclear structure observables, one could benefit only from the use of low energy Nd data below $E_{lab} \approx 30$ MeV. In the case of the low-momentum interactions which, unlike the JISP16, require the additional 3NF the final conclusions on their usefulness to study Nd scattering at higher energies could be drawn only after performing calculations taking the full Hamiltonian into account. However, the external scale of momenta given by the momentum of the incoming nucleon, which defines the relative momentum scale, imposes the limit on the energy at which the Nd elastic scattering can be investigated with the $V_{\rm low\ k}$ forces at a given cutoff Λ.

Finally, in Fig. 12 we show predictions for the differential cross section of the SST configuration in the deuteron breakup process. We observe that for all energies predictions obtained with the two lowest values of the cutoff Λ differ from ones obtained with Λ=5 fm^{-1}, which are practically indistinguishable from the CD-Bonn results. The JISP16 predictions at the two lowest energies are close to those arising from the $V_{\rm low\ k}$ with the cutoff value Λ between 1.5 and 3.0 fm^{-1}. At E=65 MeV and E=135 MeV the JISP16 model gives cross sections significantly above other results. We can conclude that, as for elastic scattering, also in the deuteron breakup we observe qualitatively similar behaviour of predictions based on the JISP16 or $V_{\rm low\ k}$ models.

VI. SUMMARY AND CONCLUSIONS

In the present work the Nd scattering process is investigated for the first time with the JISP16 NN interaction, which has already been successfully applied to nuclear structure studies. This soft interaction was constructed with the aim of incorporating genuine 3NF effects via phase-shift equivalent modifications of the 2N potential, thereby simplifying extremely complex many-body calculations of nuclear structure by reducing the need for explicit 3NFs.

The comparison of the deuteron properties for the JISP16 force and the low momentum interactions $V_{\rm low\ k}$ obtained from the CD Bonn force within the framework of unitary transformation [34], reveals the similarity of both models when the cutoff parameter $\Lambda \approx$2 fm^{-1} is used for the $V_{\rm low\ k}$ force. Thus we also studied Nd elastic scattering and the nucleon induced deuteron breakup process with the $V_{\rm low\ k}$ forces for various values of the cutoff parameter. Decreasing the cutoff parameter Λ leads to a growing importance of the induced 3N force, obtained within the renormalization group methods, when such low momentum interactions are applied in 3N structure calculations [38, 39]. Effects of such induced 3N force are significant in ^{3}H and ^{3}He bound state calculations for small values of Λ [38]. For the 3N continuum

E_{lab} [MeV]	q_0 [fm^{-1}]	$\theta^{lim}_{c.m.}(\Lambda = 1.5$ fm^{-1}) [deg]	$\theta^{lim}_{c.m.}(\Lambda = 2$ fm^{-1}) [deg]
5	0.33	180.0	180.0
13	0.53	180.0	180.0
65	1.18	78.9	115.8
135	1.70	52.3	72.0

TABLE V. The limiting c.m. angle $\theta^{lim}_{c.m.} = 2\arcsin(\frac{\Lambda}{2q_0})$, at which the momentum transfer in elastic Nd scattering at the incoming nucleon laboratory energy $E_{lab} = \frac{9}{8m}q_0^2$ becomes greater than the specified Λ value. The corresponding nucleon relative momentum is denoted as q_0 and the nucleon mass as m.

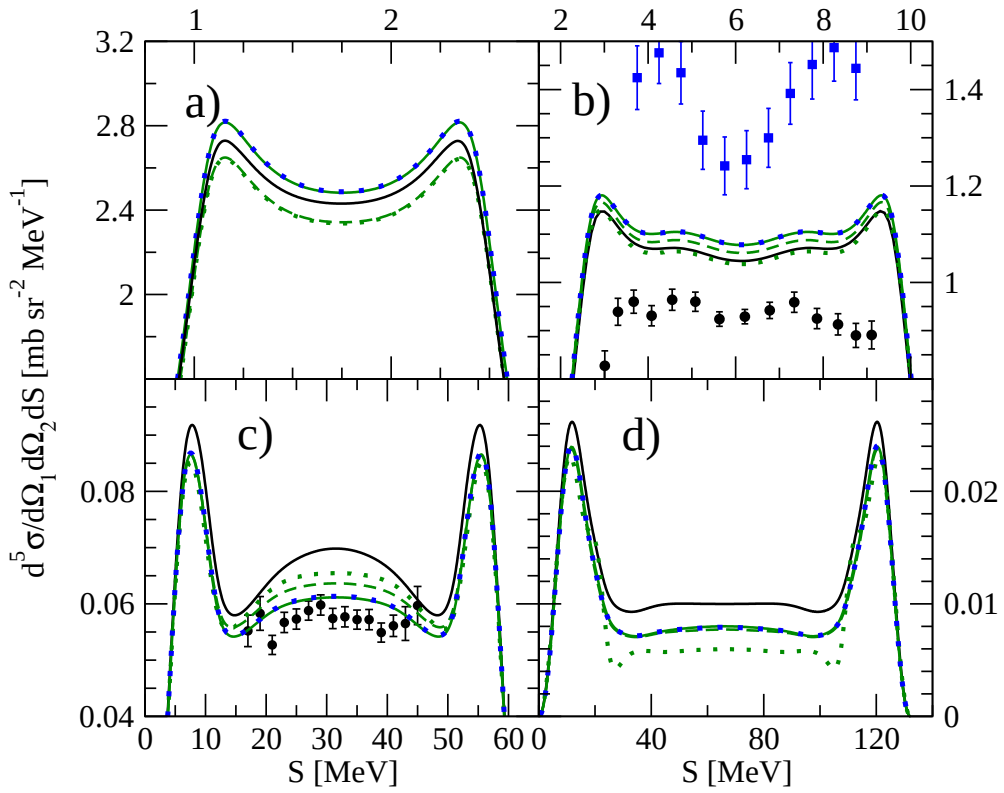

FIG. 12. (color online) The same as in Fig. 7 but for predictions based on the $V_{\text{low k}}$ interaction. Curves are as in Fig. 9 and data are as in Fig. 7.

the effects of additional 3NF related to the $V_{\text{low k}}$ force used here are rather small as shown by our comparison of low momentum interaction predictions to the CD Bonn potential results for Nd scattering observables. That conclusion is further supported by results of calculations presented in Ref. [40], where induced 3N forces have been included in 3N continuum calculations. The condition that the momentum transfers in elastic Nd scattering cannot exceed the limiting momentum Λ of the low momentum interaction restricts the application of low momentum interactions to low energies if the full scattering range is to be investigated. We have found that only for small energies of the incoming nucleon, the cutoff values in the range 1.5 fm$^{-1} \leq \Lambda < 5$ fm^{-1} can be used. At the energies equal or higher than 65 MeV the value $\Lambda = 5$ fm^{-1} delivers results equivalent to those based on the genuine CD Bonn potential.

Indeed, our results reveal that the application of the JISP16 force to a description of Nd elastic scattering should be restricted to the low energy domain, below approximately 30 MeV. In the case of the deuteron breakup the applicability of the JISP16 model depends both on the scattering energy and on the final kinematical configuration. Moreover, the P-wave components of this force require improvements because they lead to strong discrepancies with data at low energies for elastic Nd scattering observables. This is the case for the deuteron vector analyzing power, which is sensitive to the NN interaction in the P-waves. With the current version of the JISP16 force one obtains a reasonable description of the data only for some observables such as the differential cross section or the deuteron tensor analyzing power T_{21}. The description of the 3N scattering data obtained with the JISP16 model is not as satisfactory as the description of nuclear energy levels achieved with this

interaction.

Comparing the NN + 3NF results and predictions based on the two-body forces only, we cannot conclude that the JISP16 results are closer to the predictions based on the AV18 + Urbana IX potentials than results obtained from the other models of the NN interaction. So, the conclusion based on nuclear structure calculations, that the JISP16 minimizes the genuine 3NF effects must be updated with an essential addition that this is true only for some observables and at a limited range of the momentum transfer. It should be emphasized that in the nuclear structure calculations the binding energy is produced through a subtle cancellation of kinetic and potential energies while in the 3N reactions one deals with the S-matrix governed by the full potential energy. This basic difference is the reason that in the two domains of negative and positive energies the 3NF comes into play in different ways. This observation is supported by studies of 3NF effects in the 3N continuum, where the magnitude of the genuine 3NF effects seems to be small at low energies. Only when going to larger momentum transfers do the essential effects of 3NF's appear. Our results point to the possible role played by the induced 3NF when the $V_{\mathrm{low\,k}}$ force is used. It would be very interesting to check in future studies, combining a low momentum NN interaction, induced 3NF and genuine 3NF, to what extent the description of the Nd scattering observables is recovered in such a treatment.

The successful performance of the JISP16 model in the structure calculations and observed deficiencies in the scattering studies exemplify the fact that the continuum states deliver additional challenging tests of the NN potentials. They can bring out the features of the interaction which are of less importance in nuclear structure calculations. This in turn leads to a conclusion that developing future models of nuclear forces, including those derived using the inverse scattering methods, in addition to the nuclear properties, the observables in few-nucleon reactions should also be taken into account when fixing potential parameters. We plan to examine these possibilities in future improvement of a new high-quality NN force Daejeon16 [54] which reproduces observables in light nuclei without the use of 3NFs with a better accuracy than JISP16.

ACKNOWLEDGMENTS

This work is a part of the LENPIC project. It was supported by the Polish National Science Center under Grants No. DEC-2013/10/M/ST2/00420, DEC-2016/21/D/ST2/01120 and by Grant-in-Aid for Scientific Research (B) No: 16H04377, Japan Society for the Promotion of Science (JSPS). The work of AMS was supported by the Russian Science Foundation under project No. 16-12-10048. This work was also supported in part by the US Department of Energy under grant DE-FG02-87ER40371. The numerical calculations were partially performed on the interactive server at RCNP, Osaka University, Japan, and on the supercomputer cluster of the JSC, Jülich, Germany.

[1] R. Machleidt, F. Sammarruca, and Y. Song, Phys. Rev. C **53**, R1483 (1996).
[2] R. Machleidt, Phys. Rev. C **63**, 024001 (2001).
[3] R. B. Wiringa, V. G. J. Stoks, and R. Schiavilla, Phys. Rev. C**51**, 38 (1995).
[4] R. Machleidt, Nucl. Phys. **A689**, 11c (2001).

[5] R. Machleidt and D. R. Entem, Phys. Rept. **503**, 1 (2011).
[6] E. Epelbaum, H. W. Hammer, and Ulf-G. Meißner, Rev. Mod. Phys. **81**, 1773 (2009).
[7] E. Epelbaum, H. Krebs, and Ulf-G. Meißner, Eur. Phys. J. **A51**, 53 (2015).
[8] E. Epelbaum, H. Krebs, and Ulf-G. Meißner, Phys. Rev. Lett. **115**, 122301 (2015).
[9] D. R. Entem, N. Kaiser, R. Machleidt, and Y. Nosyk, Phys. Rev. C **92**, 064001 (2015).
[10] S. Binder, *et al.*, Phys. Rev. C **93**, 044002 (2016).
[11] R. Skibiński, *et al.*, Phys. Rev. C **93**, 064002 (2016).
[12] A. M. Shirokov, J. P. Vary, A. I. Mazur, and T. A. Weber, Phys. Lett. **B644**, 33 (2007).
[13] A. M. Shirokov, J. P. Vary, A. I. Mazur, S. A. Zaytsev, and T. A. Weber, Phys. Lett. **B621**, 96 (2005); J. Phys. G **31**, S1283 (2005).
[14] A. M. Shirokov, A. I. Mazur, S. A. Zaytsev, J. P. Vary, and T. A. Weber, Phys. Rev. C **70**, 044005 (2004).
[15] V. Stoks, R. Kompl, M. Rentmeester, and J. de Swart, Phys. Rev. C **48**, 792 (1993).
[16] B. R. Barrett, P. Navratil, and J. P. Vary, Prog. Part. Nucl. Phys. **69**, 131 (2013).
[17] P. Maris, J. P. Vary and A. M. Shirokov, Phys. Rev. C **79**, 014308 (2009).
[18] S. A. Coon, M. I. Avetian, M. K. G. Kruse, U. van Kolck, P. Maris and J. P. Vary, Phys. Rev. C **86**, 054002 (2012).
[19] S. A. Coon and M. K. G. Kruse, Int. J. Mod. Phys. E **25**, 1641011 (2016).
[20] A. M. Shirokov, A. G. Negoita, J. P. Vary, S. K. Bogner, A. I. Mazur, E. A. Mazur, and D. Gogny, Phys. Rev. C **90**, 024324 (2014).
[21] A. M. Shirokov, V. A. Kulikov, P. Maris, and J. P. Vary, in "NN and 3N Interactions", edited by L. D. Blokhintsev and I. I. Strakovsky. Nova Science, Hauppauge, NY, 2014, Chap. 8, p. 231, see `https://www.novapublishers.com/catalog/product_info.php?products_id=50945`.
[22] P. Maris and J. P. Vary, Int. J. Mod. Phys. E **22**, 1330016 (2013).
[23] P. Maris, A. M. Shirokov, and J. P. Vary, Phys. Rev. C **81**, 021301(R) (2010).
[24] V. Z. Goldberg, *et al.*, Phys. Lett. B**692**, 307 (2010).
[25] A. M. Shirokov, A. I. Mazur, J. P. Vary, and E. A. Mazur, Phys. Rev. C **79**, 014610 (2009).
[26] A. M. Shirokov, A. I. Mazur, E. A. Mazur, and J. P. Vary, Appl. Math. Inf. Sci. **3**, 245 (2009).
[27] A. M. Shirokov, A. I. Mazur, I. A. Mazur, and J. P. Vary, Phys. Rev. C **94**, 064320 (2016).
[28] A. M. Shirokov, G. Papadimitriou, A. I. Mazur, I. A. Mazur, R. Roth, and J. P. Vary, Phys. Rev. Lett. **117**, 182502 (2016).
[29] N. Kalantar-Nayestanaki, E. Epelbaum, J. G. Messchendorp, and A. Nogga, Rep. Prog. Phys. **75**, 016301 (2012).
[30] H. Witała, J. Golak, R. Skibiński, and K. Topolnicki, J. Phys. G: Nucl. Part. Phys. **41**, 094011 (2014).
[31] J. Golak, *et al.*, Eur. Phys. J. **A50**, 177 (2014).
[32] S. K. Bogner, *et al.*, Phys. Lett. **B576**, 265 (2003).
[33] S. K. Bogner, *et al.*, Nucl. Phys. **A784**, 79 (2007).
[34] S. Fujii, *et al.*, Phys. Rev. C **70**, 024003 (2004).
[35] A. Nogga, S. K. Bogner, and A. Schwenk, Phys. Rev. C **70**, 061002(R) (2004).
[36] S. K. Bogner, R. J. Furnstahl, and A. Schwenk, Progr. Part. Nucl. Phys. **65**, 94 (2010).
[37] T. T. S. Kuo, J. W. Holt, and E. Osnes, Phys. Scr. **91**, 033009 (2016).
[38] E. D. Jurgenson, P. Navratil, and R. J. Furnstahl, Phys. Rev. Lett. **103**, 082501 (2009).
[39] R. J. Furnstahl, and K. Hebeler, Rep. Prog. Phys. **76**, 126301 (2013).
[40] A. Deltuva, A. C. Fonseca, and S. K. Bogner, Phys. Rev. C **77**, 024002 (2008).

[41] L. E. Marcucci, A. Kievsky, L. Girlanda, S. Rosati, and M. Viviani, Phys. Rev. C **80**, 034003 (2009).
[42] B. S. Pudliner *et al.*, Phys. Rev. C **56**, 1720 (1997).
[43] W. Glöckle, The Quantum-Mechanical Few-Body Problem. Springer-Verlag, Berlin, 1983.
[44] W. Glöckle, *et al.*, Phys. Rept. **274**, 107 (1996).
[45] H. Witała, *et al.*, Phys. Rev. C **63**, 024007 (2001).
[46] `http://lib.dr.iastate.edu/energy_datasets/2/`.
[47] S. Liebig, Ulf-G. Meißner, and A. Nogga, Eur. Phys. J. **A52**, 103 (2016).
[48] S. Ōkubo, Prog. Theor. Phys. **12**, 603 (1954).
[49] K. Suzuki, Prog. Theor. Phys. **68**, 246 (1982).
[50] T. T. S. Kuo, *et al.*, Nucl. Phys. **A560**, 621 (1993).
[51] V. G. J. Stokes, R. A. M. Klomp, C. P. F. Terheggen, and J. J. de Swart, Phys. Rev. C **49**, 2950 (1994).
[52] A. M. Shirokov, V. A. Kulikov, P. Maris, A. I. Mazur, E. A. Mazur, and J. P. Vary, EPJ Web of Conf. **3**, 05015 (2010).
[53] G. Audi, A. H. Wapstra, Nucl. Phys. A**595**, 409 (1995) *and references therein.*
[54] A. M. Shirokov, I. J. Shin, Y. Kim, M. Sosonkina, P. Maris, and J. P. Vary, Phys. Lett. **B761**, 87 (2016).
[55] A. Deltuva, A. C. Fonseca, and P. U. Sauer, Phys. Rev. C **71**, 054005 (2005).
[56] K. Sagara, *et al.*, Phys. Rev. C **50**, 576 (1994).
[57] S. Shimizu, *et al.*, Phys. Rev. C **52**, 1193 (1995).
[58] H. Rühl, *et al.*, Nucl. Phys. **A524**, 377 (1991).
[59] H. Sakai, *et al.*, Phys. Rev. Lett. **84**, 5288 (2000);
H. Sakai, *et al.*, Nucl. Phys. **A684**, 577 (2001).
[60] N. Sakamoto *et al.*, Phys. Lett. **B367**, 60 (1996).
[61] J. Sowinski, D. D. Pun Casavant, and L. D. Knutson, Nucl. Phys. **A464**, 223 (1987).
[62] H. Witała, *et al.*, Few-Body Syst. **15**, 67 (1993).
[63] E. Stephan, *et al.*, Phys. Rev. C **76**, 057001 (2007).
[64] H. Mardanpour, *et al.*, Eur. Phys. J. **A31**, 383 (2007).
[65] J. Strate, *et al.*, J. Phys. G: Nucl. Phys. **14**, L229 (1988).
[66] J. Strate, *et al.*, Nucl. Phys. **A501**, 51 (1989).
[67] G. Rauprich, *et al.*, Nucl. Phys. **A535**, 313 (1991).
[68] J. Zejma, *et al.*, Phys. Rev. C **55**, 42 (1997).